Nanoscale Advances

PAPER

View Article Online
View Journal | View Issue

Cite this: *Nanoscale Adv.*, 2024, **6**, 3865

Agglomeration compaction promotes corrosion of gold nanoparticles†

Borys A. Snopok, *[a] Shavkat N. Nizamov, [b] Tetiana V. Snopok [a] and Vladimir M. Mirsky [b]

Engineered nanoparticles are increasingly being used in various areas of human activity. However, the degradation mechanism of nanobodies in harsh environments is still a puzzle for theory and experiment. We report here the results of optical spectroscopy and nanoparticle tracking analysis, quantifying agglomeration and sizing of 50 nm citrate stabilized gold nanoparticles (GNPs) in HCl solutions containing H_2O_2. The mechanism of a consecutive corrosion reaction of GNPs is discussed within the framework of the near-field approach. We found that the disappearance of single nanoparticles from a suspension does not occur due to their dissolution *per se*, but is a consequence of the formation of aggregates. The neutralization of electrostatic shielding at high ionic strength allows gold nanoparticles to approach the subnanometer distance within the region of capping defects, at which the Casimir and van der Waals attractive forces dominate. It is suggested that electric field fluctuations in the confined space between highly conductive gold nanoparticles cause complexant-stimulated loss of metal from the core in the contact area. Going beyond the charge screening limitations by constraining the reaction space and reducing the double electrical layer thickness allows for chemical processes flow along otherwise not accessible reaction pathways.

Received 3rd February 2024
Accepted 7th June 2024

DOI: 10.1039/d4na00109e

rsc.li/nanoscale-advances

1. Introduction

The nanoscale manipulation of matter is expanding the variety of natural chemical compositions with characteristics not always easily predicted from current knowledge. Moreover, quite often nanomaterials are involved in reactions which are not typical for bulk materials.[1–5] Nevertheless, engineered metal nanoparticles (EMP) are being developed and incorporated in a number of commercial products, raising the potential of human exposure during manufacture, use, and disposal. Within the nearly limitless diversity of these materials, some happen to be toxic to biological systems (*e.g.* antimicrobial properties) and environment (*i.e.* toxic pollution); others are relatively benign, while others confer health benefits (drug carriers *etc.*). A deep understanding of the nanoscale specific properties of such structures is needed to minimize possible harm caused by these materials, while supporting continued study and appropriate industrial development. The widespread and well-characterized citrate stabilized gold nanoparticles (GNP) with potent health and environmental risks are one of the best models for studying the behaviour of classical EMP in a reactive environment.[6–9]

Transformation of GNPs is a universal stage of EMP's life and important property that influences their mode of action. An EMP integration with a formation of "weakly" (association) or more "strongly" (soft agglomeration or aggregation) – bound irregular clusters as well as a release of ionic species ("leaching" of metal due to oxidative dissolution) are considered as two independent fates of metallic nanoparticles during their life cycle.[10,11] However, an elucidation of the EMP degradation mechanism in liquids is often hampered by the ambiguity in separating the contributions of complex and poorly controllable processes. Thermodynamic and kinetic stability of GNP ensembles in acidic media is as well a hot topic, since in most practical applications GNPs are often surrounded by chloride containing environment. Indeed, HCl is one of the most abundant environmental pollutants.[12,13] Chloride ion is an indispensable component of biological fluids, while hydrochloric acid in the stomach of mammals can decrease pH below 2.[14] Hydrochloric acid is widely used in industry, for example, in chemical technologies, pharmaceutical industry, food production, microelectronics, *etc.*, often in the presence of nanostructured components.[15] In some technological approaches HCl is applied in combination with hydrogen peroxide, this leads to more reactive environment owing to oxidation–chlorination process.[16] That is why in this work we study the behaviour of GNPs in aqueous solutions containing HCl also in the presence of hydrogen peroxide as an oxidizing booster.

The evolution of gold nanoparticles in chloride-containing media is not well covered in the literature, probably due to

[a]*VE Lashkaryov Institute of Semiconductor Physics, NAS of Ukraine, 41 pr. Nauki, Kyiv, 03028, Ukraine. E-mail: snopok@isp.kiev.ua*

[b]*Nanobiotechnology – Institute of Biotechnology, Brandenburg Technical University, Cottbus-Senftenberg, Universitätsplatz 1, Senftenberg, 01968, Germany*

† Electronic supplementary information (ESI) available. See DOI: https://doi.org/10.1039/d4na00109e

the mutually conflicting daily practice. An opinion on high chemical inertness of macroscopic gold samples is widespread.[17] At the same time, everyday practice indicates a high efficiency of dissolving gold nanostructures (island films, nanoparticles, *etc.*) in aqueous solutions of HCl or HCl–H_2O_2 with a formation of Au^{3+}.[18,19] Despite the degradation of gold nanoparticles in acidic chloride-containing media was repeatedly confirmed experimentally in ref. 20–26, a relationship between various stages and general mechanism of the process remains unclear. In, particular the relationship between the agglomeration (collecting in a mass of nanoparticles which does not change the phase composition of the system, *i.e.* soft agglomerates) and release of material from the metal core to the aqueous phase in the form of ions is still a puzzle for theory and experiment. To identify this relationship and establish the main route of disappearance of single nanoparticles freely moving in highly dilute suspension, we used in this work a combination of *in situ* optical spectroscopy (UV-VIS) with Nanoparticle Tracking Analysis (NTA).

The hyphenation of size-dependent NTA and nanoscale specific local plasmon resonance spectroscopy (LSPR) opens the way to direct sizing of nanobodies in liquids; this allows the characterization of both individual nanoparticles and their aggregates in undistorted form, typical for isotropic solutions. For the optimal NTA imaging of freely diffusing nanobodies, GNPs with a diameter of 50 nm were selected.[27,28] For GNPs of a given size, there is the best agreement between the equivalent spherical hydrodynamic diameter D_h of nanoparticles determined by the NTA method and the size of the metal core according to TEM data (see ESI, Fig. S1†). The choice of the concentration of hydrochloric acid and hydrogen peroxide was based on our previously obtained results.[29] Under such conditions and at a low concentration of metal nanoparticles, the reaction medium can be considered isotropic and homogeneous for optical measurements, since fluctuations in the solution density caused by gaseous reaction products can be neglected.

2. Results

2.1. Single gold nanoparticles in solution

The extinction spectrum $A(\nu)$ normalized to the quantum of light ν of very diluted (*ca.* 3×10^8 single particles of dominated size per ml according to the NTA data) GNP suspension in water is shown in Fig. 1a. Approximation of $A(\nu)/\nu$ using various profiles shows that the localized surface plasmon resonance (LSPR) band at 536 nm (18 657 cm^{-1}) is well fitted by the Lorentzian function. It differs from solutions of organic compounds, for which the Gaussian shape of the absorption band is typical. The Gaussian profile indicates that the external environment directly influences the electron transition in chromophore; in this case, averaging performs over an ensemble of chromophores that have slightly different transition energy owing to variation in their immediate environment.[30,31]

The Lorentzian profile of the extinction band means that the broadening is due to fluctuations in the characteristics of the

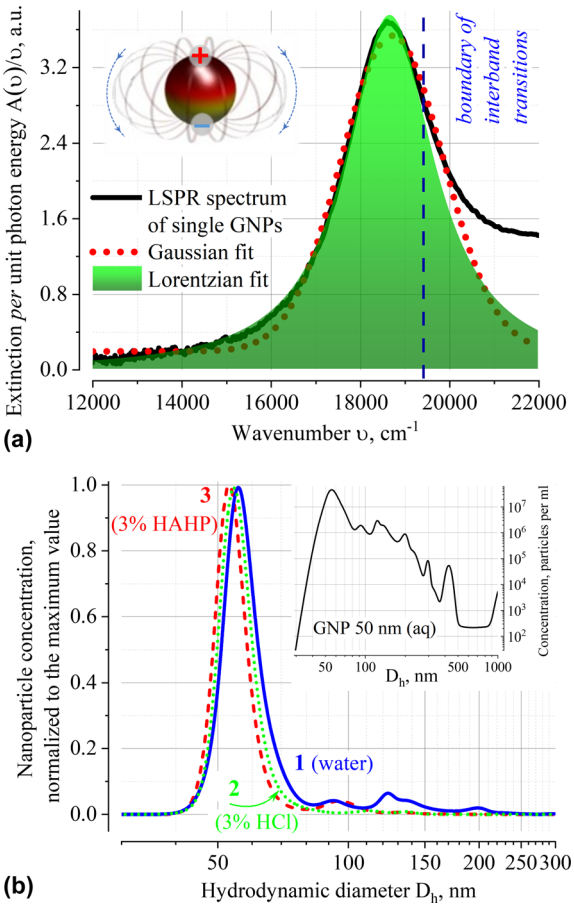

Fig. 1 Extinction spectrum normalized to the unit photon energy $A(\nu)/\nu$ of citrate stabilized GNPs 50 nm in diameter in water (concentration of single GNPs with D_h *ca.* 55 nm ~3×10^8 particles per ml) (a). The histogram of the number of particles normalized to the value at the maximum against the equivalent spherical hydrodynamic diameter of the particles D_h, obtained from NTA for suspensions of nanoparticles in water (1), 3% HCl (2) and 3% HAHP (3), respectively (b). The green fill area and the red dotted line (a) show the best approximation of the local plasmon resonance band of single nanoparticles by the Lorentzian (R-square = 0.998) and Gaussian (R-square = 0.992) profile curves. The inset in panel (b) shows the distribution for curve (1) from the panel (b) in logarithmic size scale in order to illustrate the absolute values of particle concentrations and the presence of submicron bodies within the samples. The NTA response outside the central peak is shown that the number of unidentified objects in the solution does not exceed a few percent.

transition itself (*i.e.*, dispersion of the dimensions of the metal core, presence of structural defects on the metal surface or inside the organic stabilizer layer, *etc.*), and not due to local variations in density, composition or environment temperature. The reasons for neglecting the influence of local variations of the medium on the conditions of LSPR excitation are related to the collective oscillations of electron density in plasmons and presence of an organic stabilizer that forms a uniform dielectric layer on the surface. The citrate capping is capable of damping local fluctuations in the dynamics of the solvent molecules and contributes to the constancy of the composition of the electrostatic double layer in the immediate vicinity of the nanoparticle.

The integrity of the surface layer is maintained by the process of dynamic "healing" of the arising defects by the citrate molecules present in the solution (nanoparticles are supplied as a stabilized suspension in a citrate buffer).

The position of the dominant peak in the NTA size distribution confirms that particles with a core size of ~50 nm predominate in aqueous suspension of GNP. According to the product specification, this suspension has mean hydrodynamic diameter D_h of nanoparticles in the range of 58–65 nm (Fig. 1b). No substantial shift in the position of the NTA peak of freshly prepared suspensions in different solvents (D_h = 56.0; 54.5 and 53.0 nm for distilled water, 3% HCl (aq, v/v) and 3% HAHP ((3)HCl : (3)H_2O_2 : (94)H_2O (v/v/v)) correspondingly) is observed.

2.2. GNP agglomerates in acidic suspensions

The time dependence of the extinction spectrum $A(\nu)$ of nanoparticles in 3% HCl is shown in Fig. 2a. A qualitative analysis of the spectrum shows that a decrease in the intensity of the LSPR band is accompanied by an increase in the extinction in the longer wavelength region of the spectrum. Typical deconvolution of the extinction spectra into elementary bands of the Lorentzian profile are shown in the insets of Fig. 2 (see Fig. S2, ESI† for more results). In addition to the LSPR band of single particles at 18 657 cm^{-1} (536 nm), a broad band is observed in the region of 11 000–17 000 cm^{-1} (900–600 nm). The position of the band is in good agreement with the results of other authors, who also attribute this band to irregular agglomerates/clusters/"oligomers" of gold nanoparticles.[32–40] Most likely, soft clusters consist of a few particles, since their mean hydrodynamic diameter will typically not exceed 200 nm. At t > 20 min also an absorption band at 10 500 cm^{-1} (*ca.* 950 nm) appears, which, by analogy with other researchers, can be attributed to the impact of nanoparticle aggregation in elongated geometry.[41–43]

At times above ~80 min, absorption bands in UV-VIS spectrum essentially overlap. The uncertainty of the process of deconvolution of the $A(\nu)/\nu$ spectra into elementary bands and the large residuals of the approximating functional do not allow to apply this procedure in such case. This is evidenced by the broadening of the highly constructed (complex) long-wavelength band in the region of 13 000–15 000 cm^{-1} over time (see Fig. S2, ESI†).

The NTA results (Fig. 4 and inset in Fig. 1b) confirm the presence of particles with D_h > 50 nm both in the initial suspension and over time; the presence of these particles can be associated both with soft agglomerates (100 ≤ D_h ≤ 300 nm) and very loosely connected associates (700 ≤ D_h ≤ 1000 nm) of GNPs, as well as with some foreign particles which may be present in the stock suspension of nanoparticles and in purified distilled water used to prepare the working solutions. Since the method does not allow one to establish the nature of these particles and unambiguously interpret individual peaks, below we will use only the total number of particles in the size ranges of interest which characterize the relative changes in the number of submicron particles within the indicated boundaries D_h.

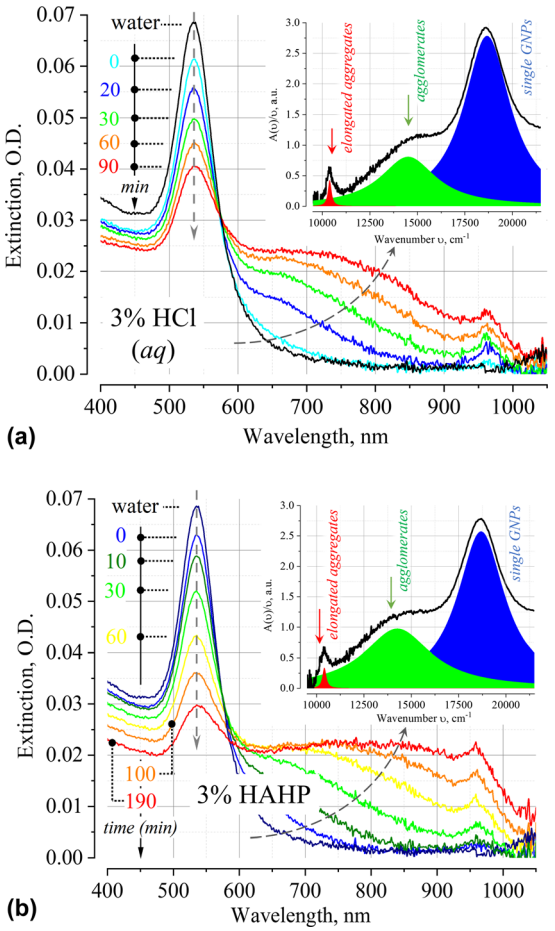

Fig. 2 Time dependence of the extinction spectra for citrate stabilized gold nanoparticles 50 nm in diameter (concentration of single GNPs with D_h *ca.* 55 nm ~3×10^8 particles per ml) in 3% HCl (aq) (a) and 3% HAHP (b) solutions. The insets show a typical deconvolution of the spectra into individual components with a Lorentzian profile for time t = 30 min after the addition of nanoparticles to the working solutions.

2.3. Nanoparticle dissolution kinetics in HCl and HAHP

Similar phenomena of the appearance of long-wavelength bands are observed in the time dependence of the extinction spectrum $A(\nu)$ of nanoparticles in both a 3% HAHP (Fig. 2b) and a 3% HCl solutions (Fig. 2a). The kinetics of spectral changes, however, are different. The dependences of the extinction value at the maximum of the single particle's LSPR band (536 nm) on time in HCl (at pH ~0.5 (3% HCl) and ~1.9) and 3% HAHP are shown in Fig. 3a. These dependences are well approximated by an exponential decay function, which describes the irreversible reduction in the number of suspended single nanoparticles in a one-step process with unique outcome (a first-order reaction whose product is clusters of nanoparticles). Within this model, the addition of hydrogen peroxide to the reaction volume (HAHP) increases the rate of this process as compared to a 3% HCl (Fig. 3a).

The NTA results confirm an increase in the number of objects in the range 100 ≤ D_h ≤ 300 nm, especially for the clusters with D_h from 90 to 130 nm, typical for soft agglomerates

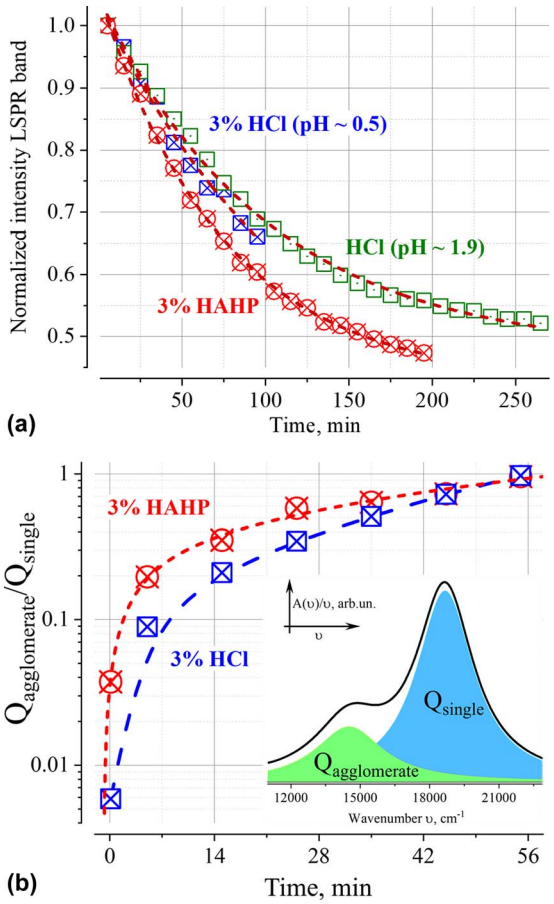

Fig. 3 Normalized value of GNP extinction at the maximum (536 nm) of the local surface plasmon resonance band of single particles *versus* time in HCl (aq) at pH 0.5 ("3%"), pH 1.9 and 3% HAHP, respectively (a). Note, that at pH less than 2 almost all ionic groups of citric acid are protonated. Ratio of agglomerates and single particles *versus* time in 3% HCl (aq) and 3% HAHP obtained from the area's ratio of the corresponding elementary Lorentz bands (see illustration in insert) (b).

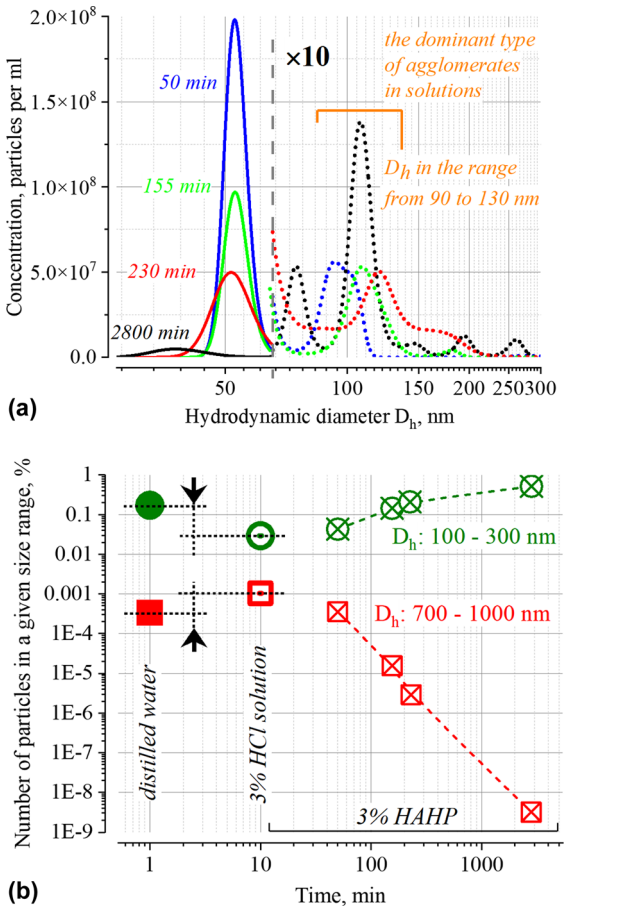

Fig. 4 Typical histograms of equivalent spherical hydrodynamic diameter of nanoparticles D_h for citrate stabilized gold nanoparticles in 3% HAHP solution for incubation time t indicated as labels on the graph (a). Dependence of the total number of particles in the ranges $100 \leq D_h \leq 300$ and $700 \leq D_h \leq 1000$ in water, 3% HCl (aq) and 3% HAHP at different incubation times (b). Green circles and red squares denote particles in medium (100–300 nm) and large (700–1000 nm) submicron size range.

of two or three particles are held together by weak physical forces. However, the particles with $D_h < 50$ nm are not detected for several hours while the peak corresponding to single particles of the initial size decreases monotonically over time (Fig. 4a). Note, that for suspensions of gold nanoparticles, NTA size detection limit is *ca.* 20 nm. So, NPs with 30–40 nm in diameter would be detected by NTA.

This observation is fundamentally important for the current work since it allows us to conclude that *the agglomeration of single particles is the dominant process of reducing the number of single nanoparticles in the suspension*. At the same time, *no decrease in the single particle size is observed in this time interval*. Similar results for silver nanoparticles were obtained in ref. 44. Broadening of the NTA peak into a region of smaller sizes than that of single particles is observed only after few hours; it is likely that these are the original dimers or trimers of particles that have already undergone significant corrosion during this time.

Also noteworthy is the growth of the submicron-sized structures ($700 \leq D_h \leq 1000$ nm, see Fig. 4b) immediately after injection of GNP into aqueous solution with pH < 2. It is not accompanied by significant changes in the UV-VIS extinction. Formation of large associates can be caused by suppression of electrostatic repulsion at low pH. Indeed, the p*K* values of carboxy group of citric acid are 3.13, 4.76 and 6.39; therefore, less than 0.3% of the total amount of these groups exposed into aqueous phase will be deprotonated at pH ~1. Notably, the number of such associates at $t > 100$ minutes decreases (Fig. 4b) while the structures with D_h ~70 and 110 nm (with concentration *ca.* (4–8) × 10^6 particles per ml, approximately 100 times less than the initial one) remain until the final stage (*ca.* 48 h) of the degradation process. Probably, in addition to single nanoparticles coated with an intact layer of organic stabilizer, some elongated aggregates are also retained. Similar architectures were observed at the final stage of degradation of gold[43] and silver nanoparticles.[45] A wide peak on the NTA distribution for a sample with an exposure time of *ca.* 2800 min (Fig. 4) indicates that only at this time the "small" objects with D_h ~30 nm (this is

close to the size detection limit of the NTA) dominate in the suspension.

2.4. Changes in populations of single particles and their aggregates over time

Deconvolution of the $A(\nu)/\nu$ spectra makes it possible to eliminate the overlap of extinction bands and directly identify changes in populations of single particles and their aggregates. The ratio of the areas of correspondent elementary bands over time is shown on Fig. 3b. It is necessary to highlight, that the addition of hydrogen peroxide leads to a faster increase in the number of aggregates. This fact indicates that some chemical transformations on the surface of nanoparticles reinforced by hydrogen peroxide booster can contribute to the process of their aggregation.

The agglomeration process is characterized by the presence of an isosbestic point, which provides evidence in favour of our assumption about a single dominate channel for the "disappearance" of GNPs (Fig. 2).[46] Indeed, the observation of isosbestic point indicates that the stoichiometry of the reaction remains unchanged over time and there is no competition between parallel reactions (such as, the dissolution of nanoparticles *etc.*) occur within the considered time range (for more details see ESI†).[47,48] Moreover, this indicates that the agglomeration products are clusters of similar composition.

Analysis of the dependence between the intensity of the LSPR band of single particles (Fig. 3a) and the ratio of agglomerates/single particles (Fig. 3b) indicates a linear correlation (Pearson coefficients > 0.98) of these values for $t \leq 60$ min (Fig. S3, ESI†). In this time interval, the intensity of the LSPR band makes it possible to quantitatively characterize the aggregation process, since its value is directly proportional to the ratio of the number of aggregated and single gold nanoparticles.

Deconvolution of the $A(\nu)/\nu$ spectra into elementary bands confirms the broadening of the extinction bands over time (Fig. 5a and b, see Fig. S2 for more details, ESI†). The strong broadening of the long-wavelength band of aggregates (Fig. 5b) is due to the growth of their configuration/composition diversity over time leads, in particular, to the formation of increasingly dense clusters.[49] Indeed, a "plasmon ruler" allows us to estimate changes in the average distance, s (Fig. 5c), between constituent nanoparticles in gold agglomerates using the shift of their resonance wavelength λ (for sub – 10 nm interparticle distances,[50–52]). Using the results of the spectra's deconvolution (Fig. S2, ESI†), the estimated average distance s monotonically decreases over time from an initial value of about 1.2 nm (5 min) to *ca.* 0.8 nm (>60 min) at a rate of about 5 pm per min for 3% HCl and *ca.* 10 pm per min for 3% HAHP at the beginning (Fig. 5c).

In the case of single particles, the weak broadening of the LSPR band (Fig. 5a) is not accompanied by a change in its position (535 ± 2 in HCl and 536 ± 2 nm in HAHP). This broadening can be caused by inevitable background level in the extinction spectra and the decomposition fitting. An overlap with another broad band or unpredictable scattering can, of course, as well change a background level. In these cases, such broadening can be neglected as a specular. However, given the low concentration of gold nanoparticles (and, accordingly,

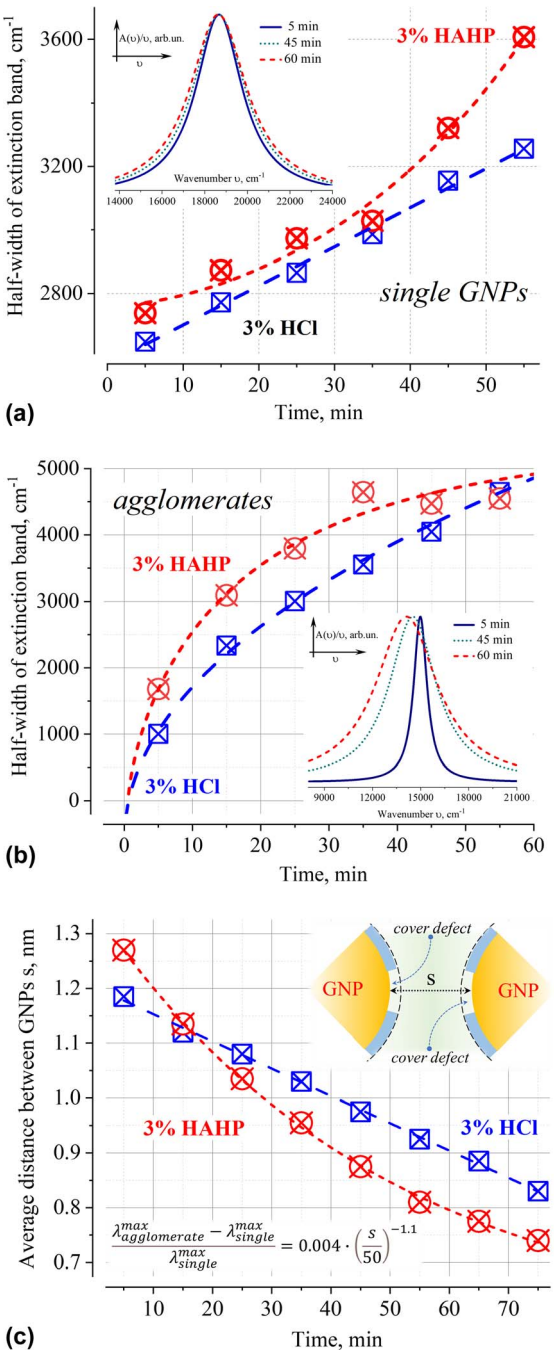

Fig. 5 Time dependence of the half-width of extinction bands of 50 nm GNPs as single particles (a) and their agglomerates (b) in 3% HCl (aq) and 3% HAHP. The average distance between nanoparticles within gold agglomerates, s, over time (c). The formula for calculation of distance between nanoparticles according to "plasmonic rulers"[50] shown in the inset (all values in nm). The presented results used the decomposition of extinction spectrum normalized to the unit photon energy $A(\nu)/\nu$ into elementary Lorentzian bands. The insets in (a) and (b) show the corresponding extinction bands in 3% HCl normalized to the maximum value to demonstrate the broadening effect.

corrosion products), and the fact that these products do not absorb/scatter in the energy range characteristic of LSPR, deconvolution was carried out for a fixed (zero optical density) baseline value.

Broadening can as well hint on some physical–chemical processes. Indeed, a slight broadening of the LSPR band is observed immediately after sample preparation: 2554, 2648 (+94) or 2738 (+184) cm^{-1} for water, HCl or HAHP respectively. The half-width of the LSPR band continued to increase further, again stronger for a more aggressive medium containing hydrogen peroxide (Fig. 5a).

In general, the LSPR resonant conditions depend on (1) the size of metal core, (2) the optical constants of the environment (Lorenz profile allow us to neglect fluctuations of this factor) and (3) the capping layer.[32,53–55] If we assume that the broadening is associated with a "symmetrical" change in the size of the metal core, then this means that the processes of gold oxidation and reduction have close efficiency under strongly acidic conditions. This seems to be an unlikely scenario owing to the high concentrations of chloride ions prevent the spontaneous formation of a metal phase, since the $AuCl^{4-}$ anion is a stable gold compound at $[H^+]$ and $[Cl^-]$ values of more than 10^{-2} M.[56]

Variations in the density/integrity of the surface coating due to its partial removal, local stacking faults, or as the result of chemical transformation as well affect the conditions of resonant excitation under near-field coupling of light. Indeed, all these defects cause local changes in the refractive index in the immediate vicinity of the surface where the electron density flows beyond the geometric boundaries of the metal nanoparticle ("spill-out effect").[57–60] The occurrence of such defects in a chlorine-containing medium is due to the adsorption of chlorine on the gold surface, which leads to a change in coordination from mono- to bidentate conformation of citric acid on the gold surface,[61] the unique capabilities of the H_2O_2–HCl (aq) system for the one-pot oxidation–chlorination of various organics[16,62] or is a consequence of the presence of steps at the intersections of the crystal lattice faces on the surface. This allows us to suggest that the broadening of the LSPR band of single nanoparticles is caused by an increase in the inhomogeneity of the organic capping layer, which causes an increase in the dispersion of the LSPR excitation conditions over time. The results in more aggressive solutions containing hydrogen peroxide confirm this suggestion – broadening is more intensively under exposure in HAHP (Fig. 5).

3. Discussion

It is generally accepted that the fate of metal nanoparticles of very different nature in reactive environment are subjected to a variety of processes: (i) redistribution of material between the cores of nanoparticles (*e.g.* Ostwald ripening in which the average particle size increases); (ii) oxidation of the metal and subsequent dissolution of the cores, while the average particle size monotonically decreases; (iii) aggregation of nanoparticles with follow-up (iv) precipitation/sedimentation. Both redistribution of the material (from smaller to larger nanoparticles) and association/aggregation are thermodynamically-controlled enthalpy-driven process tending to reduce the surface energy.[63,64] Charge and integrity of organic shell also influence on the surface energy (solvation *etc.*) as well as on the kinetics of the system evolution towards the state with a lower energy (*e.g.*, by electrostatic repulsion or Coulomb blockade of core oxidation *etc.*).[65] Therefore, the dominance of one or another process depends on the environment, pH value (*i.e.* surface potential of GNPs, *etc.*), presence of active chemical compounds (complexing or/and oxidizing agents *etc.*) capable of reacting either with stabilizer molecules or with the metal core.

3.1. A critical analysis of processes in colloidal suspensions of gold nanoparticles containing hydrochloric acid

According to the NTA and UV-VIS results, *the efficiency of spontaneous dissolution of single 50 nm citrate stabilized gold nanoparticles*, even in the presence of chloride ions at low pH values, is rather low: particles/corroded units whose size is smaller than the initial ones of single nanoparticles are observed only at the final stage of degradation of all nano-objects in suspension. This is not surprising, given the very high value of the redox potential of gold and the obstacles to the formation of oxidized gold on the surface of a citrate-stabilized nanoparticle. Indeed, even for fast electrochemically driven dissolution of much easily oxidizable silver nanoparticles, a complexation of the formed ions is required to shift reaction balance towards dissolution.[66]

Although the *Ostwald's ripening* is energetically favourable, we also consider it to be unlikely for gold nanoparticles. The reason is that it requires a consequence of few processes, at least, an oxidation of gold with a formation of soluble products diffusing in the solution up to final reduction on the larger particles. From electrochemical point of view, this process is driven by the difference in the redox potentials of small and large particles. However, the value of this potential difference between the particles of 50 nm and of infinity curvature (flat) is rather low. Moreover, a final product under similar conditions is oxidized Au^{3+} compound;[18–26,67–70] therefore, the conditions for the final reduction of the formed metallic ions into the larger NPs can hardly be achieved.

Another typical pathway of nanoparticle fate involves aggregation to form larger bodies, which often cause nanoparticle *precipitation/sedimentation*.[71] However, in the case under consideration, single particles disappear within several hours. This happens much faster than *gravitational sedimentation* which occurs for similar suspensions in the time scale of hundreds of hours.[72,73] Intensive mixing of the suspension confirms this conclusion – no changes in the spectral characteristics of suspensions were observed after mixing.

The inability to interpret experimental results within the framework of typical degradation models necessitates a more thorough analysis of the agglomeration process. Taking into account all available experimental results, it is reasonable to assume that the process of GNP dissolution goes over aggregation stage. Thus, (i) approaching of nanoparticles in aggregates follows by (ii) formation of a unique reaction space within nanoparticle clusters and, finally, (iii) activation of nanoscale specific chemical processes of gold dissolution.

3.2. Forces driving an aggregation of citrate stabilized gold nanoparticles in acidic chloride-containing media

Interaction between large dry elastic particles can be described by the repulsive Hertz-Mindlin stress model with negligible attractive forces. For capped metallic nanoparticles with a large surface area to volume ratio in suspension, a number of additional enforcements is needed. This includes (i) hydrodynamic/cohesive forces arise from particle velocity/acceleration or liquid shape; (ii) solvation/hydration/structuring forces driving interface pack around a constraining boundary; (iii) double layer forces occurring across liquids as osmotic pressure and generated by the differences in the ionic concentrations within the gap between charged objects with respect to the bulk solution;[74] (iv) short-range Casimir and van der Waals forces as well as (*v*) contact force, which is only present when the particle is sintered to another one.[75] The question is which of the known interactions between colloidal particles in solution can initiate the process of their corrosion.

A classic tool for solving issues related to the aggregation and kinetic stability of aqueous dispersions is the DLVO theory.[76,77] It takes into account the combined effect of van der Waals (at very close distances) and double layer force (at larger distances). Thus, it allows one to describe the force between charged surfaces interacting *through a liquid medium*. In kinetically stable suspensions, it is *the diffuse part of electric double layer* that separates particles and actually does not allow them to get close enough to engage in chemical reactions. The double layer force decays exponentially as a function of distance and is mainly dependent on the surface charge of the particles and *ionic strength* of the solution. The effective interaction distance is controlled by the Debye screening length which is in sub-nanometre range (*ca.* 0.5 nm, see for details in ESI†) for the solutions under consideration (*ca.* 0.36 M HCl); thus, *diffusive part of double layer force in this particular case can be neglected*. This allows us to conclude that the aggregation is a kinetically controlled process and the formation/growth of clusters is only due to the stochastic collisions of particles in solution; *high ionic strength* of the solution eliminates any long-range electrostatic interactions between nanoparticles *occurring across liquid*.

Within the concept of double layer, the first layer corresponds to the *charged surface*. As for most organic covered metallic nanoparticles, these charges originate from dissociated surface groups. At pH > 4, citric acid possessing first pK_a 3.13 is deprotonated. Thus, the citrate capping gives the gold nanoparticles a negative surface charge and GNP suspension is kinetically stable. Deprotonated citric acid has an excellent binding to the gold surface and forms strongly charged layer on the metal surface. However, when pH approached 2, almost all ionic groups are protonated and the citrate molecules are uncharged; their adsorption to the gold layer is expected to be much lower because of disappearance of mirror forces.

If electrostatic repulsion does not prevent approaching of particles and the citrate capping does not have structural defects (*i.e.*, it completely covers the surface of the metal core), a formation of low-density particle's associates possible. Weakly bound associates up to submicron size are stabilized by reducing the total surface tension and expelling excess water molecules (*i.e.*, solvation) (Fig. 4b).

If the contact of the nanoparticles is in the area of the exposed metal surface (organic coating defect), Brownian motion will push the particles closer together, *allowing the short-range attractive Casimir and then van der Waals forces to become dominant*; nanoparticles approach so close to each other that the distance between them becomes in the (sub)nanometer range (Fig. 5c).

3.3. Near-field effects in the nanogaps of metallic nanoparticles

Despite the fact that the overwhelming majority of publications are devoted to light induced interactions between plasmonic nanoparticles, an association and agglomeration of nanoparticles proceed also in the dark. Therefore, the discussed here interactions do not imply external stimulation, in particular, by light.

When metal particles approach to a distance of tens of nanometers, a Casimir (at larger nanoscale distances) and then van der Waals forces (at very close distances) arises between them. The Casimir force is the strongest force acting on two uncharged conducting objects separated by confined space gaps in nanometer range due to the restructuring of the quantum vacuum fluctuations of a field.[78–80] Moreover, it was shown that the Casimir interaction between two objects of the same material results in *passive Casimir trapping* so that two objects can remain *without contact at a specific distance* (Casimir equilibrium).[81] With further approach of uncharged metal particles without own dipole moments, dispersion interactions caused by van der Waals forces begin to dominate at sub-nanometer distances.[82,83]

It was found that for the system of two spherical shelled nanoparticles interaction potential is similar to the well-known Lennard-Jones potential where the overall two-body contribution yields an attractive interaction.[84,85] These forces are caused by fluctuations of electrons and quantum fluctuations whose spectrum is altered by the presence of boundaries.[86–88] It is reasonable to stress that according to theoretical calculations, the light-induced interaction for strongly focused laser beams becomes comparable in strength to the action of Casimir force.[89] When the nonlinear polarizability of nanoparticles is also taken into account, an additional interaction appears, leading to the attractive ponderomotive forces in the system of two nanoparticles.[90] *Thereby, an interaction of metal nanoparticles does not require a presence of light for sure, but is limited by the possibility to approach to the distance at which near-field effects can manifest*. In our case due to the small Debye length and defects in the organic coating layer, nanoparticles can approach each other to the sub-nanometer distance (Fig. 5).

Since the stochastically oscillated local fields play an important role in the near-field, their spatial distribution leads to the formation of local electrostatic gradients. In the nanogaps the electric field distribution depends on the number, size and mutual arrangement of constituent nanoparticle aggregate; configurations can arise in which nanoparticles can both

compensate or even suppress each other's action, and, conversely, significantly enhance the local fields in the nanogaps.[32,40,78,89,91–93]

To summarize, we can conclude that the aggregation of nanoparticles in solutions with sub-nanometer Debye length is caused by fluctuations-based near-field electrostatic interactions. In this case the "unusual" chemical reactions can occur within the confined space between closely approached nanoparticles. This conclusion is in good agreement with the results of other authors, who showed that the gold nanoparticles exhibited different dissolution behaviors as ensembles compared to the single particles.[94] Similar results were obtained for polycrystalline films, which showed that surface corrugations induce fluctuating near-field variation and modulate corrosion reaction.[29,92]

The corrosion resistance of gold under normal conditions is caused by the high standard potential of this material.[17,95] However, the high energy required for the oxidation can be lowered by decreasing of the energy of gold ions in the aqueous phase. This can be achieved by complexation (decrease of the chemical component of electrochemical potential), addition of oxidizers such as hydrogen peroxide (to reduce the electrode potential of gold) and by application of electric field (decrease of the electrical component of electrochemical potential). The second well known effect of the electric field is the influence on the activation energy of this process. The formation of a complex also reduces the energy consumption for detachment of surface gold atoms due to the redistribution of the electron density of the complexing agent, which weakens the bonds that fix the atom in the crystal lattice. Therefore, we can suggest that the high concentration of chloride ions and the presence of high electric field within the nanogap can promote local corrosion of metal in nanoparticles in the area of their contacts. The anticipated corrosion mechanism is similar to oxidative intergranular or crevice dissolution of metals in polar solutions of halogens occurring at high fluctuations of local electric field in confined space.[96]

3.4. The irreversible consecutive mechanism for the degradation of gold nanoparticles in acidic aqueous suspensions

The analysis of obtained experimental results and their interpretation within the framework of the near-field approach indicates that the corrosion of gold nanoparticles in chlorine-containing medium is a multistage process. It includes the partial destruction of the stabilizer layer in acidic conditions, which in turn leads to the closest agglomeration of GNPs, which are consecutively dissolved in the area of interparticle contacts (Fig. 6). This process is more intensive in the presence of hydrogen peroxide, which provides strong oxidation conditions for capping agents and reduce electrode potential of gold at acidic pH. As the metal phase dissolves within the strongly confined space of the nanogaps, a part of the agglomerates can transform into stable capped "clusters" through oriented attachment in a common crystallographic alignment. Similar elongated structures are observed at the initial stages of synthesis of nanostructures (nuclei line up in chains due to the features of the crystal structure of gold[97] or silver[45]); potentially

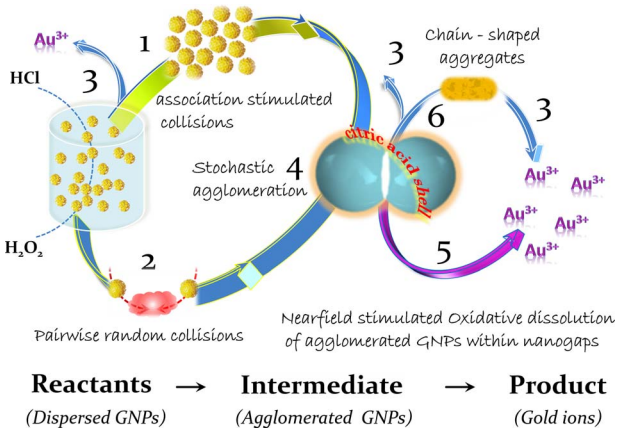

Fig. 6 Proposed mechanism of multistep degradation of gold nanoparticles in acidic chloride – containing aqueous suspensions. The process (1) illustrates a weak association of GNPs in acidic conditions when their surface charge is decreasing. It is followed by stochastic agglomeration, where contact occurs in places of defects in organic coatings (2). Driven by Casimir and van der Waals forces, stronger soft aggregates are gradually formed (4). Through complexation under high fluctuations of local electric fields in confined space and Au ions transfer to the aqueous phase, a gold within nanogap is dissolved from metal core (5). The process (6) represents a potential formation of elongated aggregates through oriented attachment in a common crystallographic alignment. The process (3) is an oxidative dissolution of metal on the surface of single nanobodies (slow process).

the same architectures are ones of the most "long-lived" in the process of GNP degradation (Fig. 4).

4. Experimental

4.1. Chemicals and reagents

Chemicals (hydrochloric acid) (HCl, 37%, Roth 9277-1, 1.19 g ml^{-1}), hydrogen peroxide (H_2O_2, 30%, Roth) and gold nanoparticles (the stock solution Aldrich 741 957 (10 nm); Aldrich 741 965 (20 nm); Aldrich 741 973 (30 nm); Aldrich 741 981 (40 nm); Aldrich 742 007 (50 nm); Aldrich 742 015 (60 nm); Aldrich 742 023 (80 nm); Aldrich 742 031 (100 nm); Aldrich 742 866 (200 nm)) were purchased from the above commercial suppliers and were used without further purification. All solutions were prepared according to the standard procedures using Milli-Q-purified water.

HCl working solution, was prepared by dissolving of 3 ml of hydrochloric acid (HCl, 37%) in 97 ml of distilled water leading to referred to below as "3% HCl" solution with pH ~ 0.5 (0.36 M). Water solutions of hydrochloric acid and hydrogen peroxide (HAHP) were prepared by mixing of 3 ml of hydrochloric acid (HCl, 37%), 3 ml aliquots of hydrogen peroxide (H_2O_2, 30%) and 94 ml of distilled water; in this case the volumetric ratio was (x) HCl : (x)H_2O_2 : (100 − 2x)H_2O (v/v/v) for $x = 3$ (referred to below as "3% HAHP" solution). Notable, if $x > 3$, the bubbles of gaseous reaction products were generated both in the bulk of the solution and on the glass surface of the cuvette during the dissolution of gold; the bubbles can create local variations in the concentration of active components and may lead to a non-

uniform condition for chemical conversions as well disturb measurement owing to additional light scattering at the solution/bubble/glass interfaces.

Working samples of GNPs were prepared from the stock suspension (Aldrich 742 007) immediately before measurements by 1 : 15 dilution by water or above-described aqueous solutions of HCl or HAHP *in glass vials*. The concentrations of the single GNP of dominant size (maximum of NTA distributions at $D_h = 56$ nm) after preparation were $\sim 3 \times 10^8$ particles per ml, the mean hydrodynamic diameter of nanoparticle D_h according to NTA measurements was 56 nm. The samples *in glass vials* were stored in the dark using aluminium foil to prevent a possible light exposure. Thus, irradiation (low intensity, capturing about 2% of the suspension volume) occurred only during spectrum measurement (scanning range 200–1100 nm, scanning time 5 min). The experiments were performed at 21 ± 1 °C.

4.2. Characterization methods: optical measurements

The UV-VIS spectra of samples were recorded using Evolution 220 spectrometer (Thermo Scientific, Germany). The spectra were recorded using a *glass cuvette* (10 mm, QG Precision Cells, 6030-10-10, Hellma Analytics) with the same solvent as a reference; an interval of 10 minutes was used for kinetic analysis. Totally up to 20 scans were collected for each measurement with a resolution of 2 cm^{-1}.

4.3. Characterization methods: nanoparticle tracking analysis (NTA)

Direct visualization, sizing and counting of suspended GNPs was performed using a NanoSight™ NS300 Nanoparticle Analysis System (Malvern Panalytical Ltd, Malvern, Worcs, UK https://www.malvernpanalytical.com) equipped with a homemade injection system based on automatic autosampler (for details see Fig. S3, ESI†).

Before measurements the water carrier for suspensions of GNP were filtered through 0.2 μm filter (Millipore). Between experiments, the system was flushed with a large volume of filtered water at a high flow rate (up to 2 ml min^{-1}). Scattered light from the suspended nanoparticles interrupting the green (532 nm) laser beam passing through the sample chamber was recorded as a video file of the particles undergoing Brownian motion. Camera focus, gain and shutter settings were adjusted in unison to generate optimally exposed blur-free images of particles and a capture duration of 60 s was employed. Image processing was done in standard mode for 5 repetitions with all other analysis parameters set to recommended default values.

Data analysis was performed using the software provided by the manufacturer (NanoSight NTA software version 3.4, Build 3.4.4), no additional initial data conversions or calculations were performed. The results of the analysis are presented as a histogram of the number of particles of a given size against the equivalent spherical hydrodynamic diameter of the particles D_h, calculated on the basis of the measured change in the position of the particle using the Stokes–Einstein equation. Estimations of viscosity of HCl and H_2O_2 solutions based on linear approximation of data[98,99] indicate that the difference of used solutions of HCl and HAHP from pure water is ~2%; therefore, viscosity of pure water was used in the calculation of D_h.

In order to minimize the systematic errors caused by the peculiarities of the implementation of the NTA method,[28] the D_h value of commercially available gold nanoparticles was measured in the range of 20–200 nm. The results are presented in Fig. S1, ESI†. Considering that in this work we are interested in changes in the initial size of GNPs, particles with a diameter of ~50 nm were selected. According to the results of inter-laboratory testing presented in ref. 28, the hydrodynamic diameter D_h of these nanoparticles best corresponds to the size of nanoparticles obtained using transmission electron spectroscopy (determining the size of the metal core d), taking into account the thickness of the organic stabilizer layer (less than 1 nm).[61,100] Notably, nanoparticles with a diameter of 50 nm are located in the center of the linear part of the dependence of D_h *versus* d (Fig. S2, ESI†), ensuring the correct registration of changes in the size of individual nanoparticles. For a qualitative assessment of the number of submicron particles in a certain range of D_h, integral values were calculated, *i.e.* the total number of particles whose hydrodynamic diameter was in the ranges $100 \leq D_h \leq 300$ and $700 \leq D_h \leq 1000$ nm.

4.4. Data processing of GNP extinction spectra

The extinction of individual spherical gold particles is caused by the processes of absorption and coherent scattering (changing the angular distribution) of light. In the basic Mie theory, the expected contour of the extinction band under the local surface plasmon resonance conditions is described by Lorentzian function including both equilibrium (plasma oscillations) and nonequilibrium (inter-band transitions) free charge carriers.[32,33]

The shape of a suspension extinction spectrum is the result of the summation of a large number of spectra of individual nanoparticles. In order to match the statistical theoretical models (formulated in terms of the number of particles of a given property) and the measured spectra, it is necessary to represent the extinction band as a result of cumulative behaviour of nanoparticles sets with a given energy. In order to move into a probabilistic representation of optical spectra, the concept of Einstein coefficients is usually used: the Einstein coefficients are quantities describing the probability of electron transition per unit frequency (light quantum).[30,31,101–103] To obtain a value directly proportional to the corresponding Einstein coefficient, it is necessary to divide the extinction spectrum $A(\nu)$ to the value of the quantum energy ν (*e.g.* wavenumber); in this case, the random variable $A(\nu)/\nu$ does not more depend on the transition energy and its quantity is proportional to *the number of particles* having electron transition with a given quantum energy ν. This procedure is widely used in molecular spectroscopy and photovoltaics.[101–103]

Deconvolution of the $A(\nu)/\nu$ spectrum by individual symmetrical components makes it possible to improve resolution and identify a particular band shape specific for the corresponding electronic processes.[30,31,104,105] The shape of the

band indicates the dominant broadening mechanism.[106–108] If the broadening is due to fluctuations of the transition moment itself (intrinsic properties), the band profile is described by the Lorentzian curve. If the influence of the external environment dominates, *i.e.* due to a presence of other objects close to the absorber, an inhomogeneous thermal (or proximity) broadening is observed which results in a Gaussian absorption band profile.

The procedures of Origin (OriginLab Corporation) were used for spectra deconvolution and analysis.

5. Conclusion

Near-field engineering utilizing local fields can drive chemical reactions along otherwise not accessible reaction pathways. Many approaches based on manipulation of photon energy flow in plasmonic chemistry have been proposed and practically implemented, including near-field etching,[109] photooxidative dissolution of gold,[110] near-field assisted chemical reactions,[90,111,112] and the generation of localized magnetic field.[113] Here we would like to draw attention to the fact that *atypical reaction pathways can be activated also without optical excitation*. We demonstrate that near-field assisted chemical transformation proceeds as well in darkness, given that GNPs able to come very close to each other.

In the search for nanoscale specific effects of transformation of metallic nanoparticles it usually assumed that particle agglomeration can result in reduced near-field effects.[114] This is explained by a decrease of the free surface/volume ratio. In this study, we argue that closest agglomeration paves also the way for unique nanogap-based reactors with otherwise hidden near-field effects. In such strongly confined space between conducting boundaries chemical processes are activated and enhanced by fluctuating local electrostatic field in Casimir or van der Waals bound nanostructures.

One of the most important practical takeaways of this report is that the integrity of the capping coating of gold nanoparticles is the key factor determining their behaviour in chloride-containing media. Despite the fact that a number of authors emphasize the problem,[115–117] the implications of coating breakdown are often vainly overlooked. It can be of a great importance, for instance, when examining GNP applicability in biological liquids where the thickness of the diffuse part of double layer is often less than 1 nm under physiological conditions.[118] As shown in this work, chemically induced defects in the coating of nanoparticles can promote the dissolution of the metal in nanogaps and ultimately lead to the disappearance of the nanocarrier. Having ways to maintain the kinetic stability of gold nanoparticle suspensions in different environments is a prerequisite, for example, for the development of pharmaceuticals using GNP based formulations intended for oral administration, or the successful application of a new type of plasmonic nanoparticle etching-based optical sensors.[119]

It is also important to emphasize that the degradation of nanostructured metals is a multiscale consecutive reaction in which structural transformations and chemical reactions are mutually coordinated through stochastic processes of transport of objects whose mass differs by 7–8 orders of magnitude (aggregates, particles and ions). *In this case, some new functional architectures built from the initially inert elements acts as a nanoreactors (temporal intermediate), those newly acquired properties open the way for the implementation of the "unusual" chemical transformations*. Thus, in contrast to homogeneous processes in isotropic solutions an evolution of colloidal nanosystems is influenced by their spatial (self)organization and exhibit typical features of complex systems.[120–122]

The results obtained in this work focus the reader's attention on near-field processes specific for Casimir or van der Waals bound nanostructures,[123–128] in particular, transformation in agglomerates of metal nanoparticles in chloride-containing media. This knowledge is important for risk assessment and product development in industry and pharmacology assuming their potential threats to environmental health and safety risks. Clearly understood mechanisms, integrity limits and conditions under which a GNP's protective capping fails, opens the ways for conscious and purposeful development of task-oriented stable nanomaterials to derive the benefits of nanoscale-based technologies while limiting adverse health impacts or industrial mismatch.

Author contributions

Conceptualization, B. S. and V. M.; methodology, B. S. and S. N.; software, S. N.; formal analysis, B. S. and T. S.; investigation, B. S.; resources, S. N. and T. S.; data curation, B. S. and T. S.; writing—original draft preparation, B. S.; writing—review and editing, V. M. and S. N.; visualization, B. S. and T. S.; project administration, V. M.; funding acquisition, V. M. All authors have read and agreed to the published version of the manuscript.

Conflicts of interest

There are no conflicts of interests to declare.

Acknowledgements

Authors thanks DFG-Projekt – GZ: MI 599/12-1 and DAAD (B. S., Grant 57507440) for support this work. This work has received as well funding through the MSCA4Ukraine project (Grant ID 1119494), which is funded by the European Union.

Notes and references

1 R. Abbasi, G. Shineh, M. Mobaraki, S. Doughty and L. Tayebi, *J. Nanopart. Res.*, 2023, **25**, 43.
2 L. Li and Y. J. Zhu, *J. Colloid Interface Sci.*, 2006, **303**(2), 415–418.
3 A. L. Suherman, G. Zampardi, S. Kuss, E. E. L. Tanner, H. M. A. Amin, N. P. Young and G. Richard, *Phys. Chem. Chem. Phys.*, 2018, **20**, 28300.
4 B. Snopok and O. Snopok, in *NATO Science for Peace and Security Series A: Chemistry and Biology, Advanced*

Nanomaterials for Detection of CBRN, ed. J. Bonca and S. Kruchinin, Springer, Nature, B.V, 2020.
5 C. Girard, C. Joachim and S. Gauthier, *Rep. Prog. Phys.*, 2000, **63**, 893.
6 S. J. Amina and B. Guo, *Int. J. Nanomed.*, 2020, **15**, 9823.
7 A. Sani, C. Cao and D. Cui, *Biochem. Biophys. Rep.*, 2021, **26**, 100991.
8 R. Stein, B. Friedrich, M. Mühlberger, N. Cebulla, E. Schreiber, R. Tietze, I. Cicha, C. Alexiou, S. Dutz, A. R. Boccaccini and H. Unterweger, *Molecules*, 2020, **25**, 4425.
9 X. Hu, Y. Zhang, T. Ding, J. Liu and H. Zhao, *Front. Bioeng. Biotechnol.*, 2020, **8**, 990.
10 S. McCarrick, K. Midander, M. Krausová, U. Carlander and H. L. Karlsson, in the Presence of Human Macrophages, *Int. J. Nanomed.*, 2021, **16**, 5895.
11 M. Z. Iqbal, I. Ali, W. S. Khan, X. Kong and E. Dempsey, *Mater. Des.*, 2021, **205**, 109694.
12 C. D. Evans, D. T. Monteith, D. Fowler, J. N. Cape and S. Brayshaw, *Environ. Sci. Technol.*, 2011, **45**(5), 1887.
13 I. V. Kruglenko and B. A. Snopok, *Theor. Exp. Chem.*, 2018, **54**, 53.
14 O. Mbanga, E. Cukrowska and M. Gulumian, *J. Nanopart. Res.*, 2021, **23**, 29.
15 V.-P. Thai, H. D. Nguyen, N. Saito, K. Takahashi, T. Sasaki and T. Kikuchi, *Nanoscale Adv.*, 2022, **4**, 4490–4501.
16 G. I. Nikishin, N. I. Kapustina, L. L. Sokova, O. V. Bityukov and A. O. Terent'ev, *Tetrahedron Lett.*, 2020, **61**, 152154.
17 S. Cherevko, A. A. Topalov, A. R. Zeradjanin, I. Katsounarosa and K. J. J. Mayrhofer, *RSC Adv.*, 2013, **3**, 16516.
18 H. Shi, H. Bi, B. Yao and L. Zhang, *Appl. Surf. Sci.*, 2000, **161**, 276.
19 S. R. King, J. Massicot and A. M. McDonagh, *Metals*, 2015, **5**, 1454.
20 S. K. Misra, A. Dybowska, D. Berhanu, S. N. Luoma and E. Valsami-Jones, *Sci. Total Environ.*, 2012, **438**, 225.
21 J. Hedberg, E. Blomberg and I. O. Wallinder, *Environ. Sci. Technol.*, 2019, **53**(8), 4030.
22 H. Shi, H. Bi, B. Yao and L. Zhang, *Appl. Surf. Sci.*, 2000, **161**(1–2), 276.
23 M. N. Martin, A. J. Allen, R. I. MacCuspie and V. A. Hackley, *Langmuir*, 2014, **30**(38), 11442.
24 S. Riaz, L. Qu, E. K. Fodjo, W. Ma and Y.-T. Long, *RSC Adv.*, 2014, **4**, 14031.
25 J. R. Reimers, M. J. Ford, A. Halder, J. Ulstrup and N. S. Hush, *Proc. Natl. Acad. Sci. U. S. A.*, 2016, **113**(11), E1424.
26 S. K. Tripathy, J. Y. Woo and C.-S. Han, *Anal. Chem.*, 2011, **83**(24), 9206.
27 *Product Specification Product Number: 742007 "50 Nm Diameter, OD 1, Stabilized Suspension in Citrate Buffer"*, **https://www.sigmaaldrich.com/UA/en/product/aldrich/742007**.
28 S. M. Briffa, J. Sullivan, A. Siupa, P. Carnell-Morris, M. Carboni, K. Jurkschat, R. J. B. Peters, C. Schultz, K. H. Seol, S. J. Kwon, S. Park, T. H. Yoon, C. Johnston, S. Lofts and E. Valsami-Jones, *J. Visualized Exp.*, 2020, **164**, e61741.
29 B. Snopok, A. Laroussi, C. Cafolla, K. Voïtchovsky, T. Snopok and V. M. Mirsky, *Surf. Interfaces*, 2021, **22**, 100818.
30 B. A. Snopok and Ya. D. Lampeka, *Opt. Spectrosc.*, 1992, **73**(4), 400.
31 B. A. Snopok and Y. D. Lampeka, *Opt. Spectrosc.*, 1993, **75**(2), 189.
32 V. Klimov, *Nanoplasmonics*, Jenny Stanford Publishing, 2014.
33 I. M. Krishchenko, É. G. Manoilov, S. A. Kravchenko and B. A. Snopok, *Theor. Exp. Chem.*, 2020, **56**, 67.
34 Y. Liu, W. Fu, Z. Xu, L. Zhang, T. Sun, M. Du, X. Kang, S. Xiao, C. Zhou, M. Gong and D. Zhang, *Front. Chem.*, 2021, **9**, 675491.
35 V. A. Dhumale, R. K. Gangwar, S. S. Datar and R. B. Sharma, *Mater. Express*, 2012, **2**(4), 311.
36 E. Moaseri, J. A. Bollinger, B. Changalvaie, L. Johnson, J. Schroer, K. P. J. Orcid and T. M. Truskett, *Langmuir*, 2017, **33**(43), 12244.
37 S. Shrestha, B. Wang and P. Dutta, *Adv. Colloid Interface Sci.*, 2020, **279**, 102162.
38 B. D. Dana, A. N. Koya, X. Song and J. Lin, *Phys. B*, 2022, **631**, 413706.
39 M. Loumaigne, C. Midelet, T. Doussineau, P. Dugourd, R. Antoine, M. Stamboul, A. Débarrecd and M. H. V. Werts, *Nanoscale*, 2016, **8**(12), 6555.
40 Y. Zhou, J. Zhu, J. Xi, K. Li and W. Huang, *J. Phys. Chem. A*, 2023, **127**(1), 390.
41 X. Gu, V. Timchenko, Y. G. Heng, L. Dombrovsky and R. Taylor, *Appl. Sci.*, 2018, **8**(7), 1132.
42 L. V. Melendez, S. J. Barrow, A. Liu, T. U. Connell and D. E. Gómez, *Optica*, 2020, **7**, 1666.
43 W. Wei, R. Gou, C. Shu and Z. Guo, *J. Phys. Chem. C*, 2023, **127**(16), 7808–7815.
44 J. L. Axson, D. I. Stark, A. L. Bondy, S. S. Capracotta, A. D. Maynard, M. A. Philbert, I. L. Bergin and A. P. Ault, *J. Phys. Chem. C*, 2015, **119**(35), 20632.
45 I. Fernando and Y. Zhou, *Chemosphere*, 2019, **216**, 297.
46 F. Kaspar, *ChemBioChem*, 2023, **24**, e202200744.
47 *Compendium of Chemical Terminology*, ed. A. D. McNaught and A. Wilkinson, IUPAC the "Gold Book", Blackwell Scientific Publications, Oxford, 2nd edn, 1997.
48 E. H. Mohamed, H. M. Lotfy, M. A. Hegazy and S. Mowaka, *Chem. Cent. J.*, 2017, **11**, 43.
49 J. H. Yoon, F. Selbach, L. Schumacher, J. Jose and S. Schlücker, *ACS Photonics*, 2019, **6**(3), 642.
50 G. A. Kelesidis, D. Gao, F. H. L. Starsich and S. E. Pratsinis, *Anal. Chem.*, 2022, **94**(13), 5310.
51 R. T. Hill, J. J. Mock, A. Hucknall, S. D. Wolter, N. M. Jokerst, D. R. Smith and A. Chilkoti, *ACS Nano*, 2012, **6**(10), 9237.
52 X. Ma, Y. Guo, M. Pu, X. Li and X. Luo, *Plasmonics*, 2019, **14**, 845.
53 S. Manzhosa, G. Giorgib, J. Lüderd and M. Ihara, *Adv. Phys.: X*, 2021, **6**(1), 1908848.

54 L. Cheng, G. Zhu, G. Liu and L. Zhu, *Mater. Res. Express*, 2020, **7**(12), 125009.
55 J. Shin, M. Song, H. Hafeez, P. J. Jeusraj, D. H. Kim, J. C. Lee, W. H. Lee, D. K. Choi, C. H. Kim, T. S. Bae, S. M. Yu, K. Kim, H. G. Park, K. B. Chung, A. Song, Y. C. Kang, J. Park, C. Kim and S. Ryu, *Org. Electron.*, 2019, **66**, 94.
56 I. V. Mironov, *Medium Effects and Complexation in the Electrolyte Solutions*, Novosibirsk, SB RAS, Institute of Inorganic Chemistry, 2003.
57 R. Javed, A. Sajjad, S. Naz, H. Sajjad and Q. Ao, *J. Mol. Sci.*, 2022, **23**, 10521.
58 S. J. Zalyubovskiy, M. Bogdanova, A. Deinega, Y. Lozovik, A. D. Pris, K. H. An, W. P. Hall and R. A. Potyrailo, *J. Opt. Soc. Am. A*, 2012, **29**, 994.
59 A. Bonyár, *Biosensors*, 2021, **11**(12), 527.
60 L. Guo, J. A. Jackman, H.-H. Yang, P. Chen, N.-J. Cho and D.-H. Kim, *Nano Today*, 2015, **10**(2), 213.
61 D.-B. Grys, B. de Nijs, A. R. Salmon, J. Huang, W. Wang, W.-H. Chen, O. A. Scherman and J. J. Baumberg, *ACS Nano*, 2020, **14**(7), 8689.
62 G. I. Nikishin, N. I. Kapustina, L. L. Sokova, O. V. Bityukov and A. O. Terent'ev, *Tetrahedron Lett.*, 2020, **61**(31), 152154.
63 N. T. K. Thanh, N. Maclean and S. Mahiddine, *Chem. Rev.*, 2014, **114**, 7610.
64 A. A. Eliseev and A. V. Lukashyn, in *Functional Nanomaterials*, ed. Y. D. Tretyakov, Fizmatlyt, Moscow, 2010.
65 M. Z. Iqbal, I. Ali, W. S. Khan, X. Kong and E. Dempsey, *Mater. Des.*, 2021, **205**, 109694.
66 S. Nizamov, O. Kasian and V. M. Mirsky, *Angew. Chem., Int. Ed.*, 2016, **55**(25), 7247.
67 H. Shi, H. Bi, B. Yao and L. Zhang, *Appl. Surf. Sci.*, 2000, **161**(1–2), 276.
68 S. McCarrick, K. Midander, M. Krausová, U. Carlander and H. L. Karlsson, *Int. J. Nanomed.*, 2021, **16**, 5895.
69 U. Carlander, K. Midander, Y. S. Hedberg, G. Johanson, M. Bottai and H. L. Karlsson, *ACS Appl. Bio Mater.*, 2019, **2**(3), 1006.
70 K. Oya, K. Aoshika, M. Ageishi, H. Magara, S. Ogawa, Y. Takakuwa and T. Takami, *Chem. Lett.*, 2021, **50**, 191.
71 C. M. Alexander, J. C. Dabrowiak and J. Goodisman, *J. Colloid Interface Sci.*, 2013, **396**, 53.
72 J. Midelet, A. El-Sagheer, T. Brown, A. G. Kanaras and M. H. V. Werts, *Part. Part. Syst. Charact.*, 2017, **34**(10), 1700095.
73 C. M. Alexander, J. C. Dabrowiak and J. Goodisman, *J. Colloid Interface Sci.*, 2013, **396**, 53.
74 J. N. Israelachvili, in *Intermolecular and Surface Forces*, Elsevier eBooks, 2011.
75 S. C. Endres, L. C. Ciacchi and L. Mädler, *J. Aerosol Sci.*, 2021, **153**, 105719.
76 V. A. Hernández, *ChemTexts*, 2023, **9**, 10.
77 B. Derjaguin and L. Landau, *Acta Phys.-Chim.*, 1941, **14**, 633.
78 T. Gong, M. R. Corrado, A. R. Mahbub, C. Shelden and J. N. Munday, *Nanophotonics*, 2021, **10**(1), 523.
79 E. Marino, O. A. Vasilyev, B. B. Kluft, M. J. B. Stroink, S. Kondrat and P. Schall, *Nanoscale Horiz.*, 2021, **6**, 751.
80 J. R. Villanueva-Valencia, H. Guo, R. Castañeda-Priego and Y. Liu, *Phys. Chem. Chem. Phys.*, 2021, **23**, 4404.
81 R. Zhao, L. Li, S. Yang, W. Bao, X. Yang, P. Ashby, Y. Wang and X. Zhang, *Science*, 2019, **364**, 984.
82 S. Y. Buhmann, Dispersion Forces I, Macroscopic Quantum Electrodynamics and Ground-State Casimir, *Casimir-Polder and van der Waals Forces*, Springer-Verlag, Berlin, Heidelberg, 2012.
83 C. Girard, C. Joachim and S. Gauthier, *Rep. Prog. Phys.*, 2000, **63**(6), 893.
84 H. Demchenko and N. Rusinchuk, *J. Nanotechnol.*, 2019, 4270454.
85 V. Lozovski and V. Piatnytsia, *J. Comput. Theor. Nanosci.*, 2013, **10**, 2288.
86 H. B. G. Casimir and D. Polder, *Phys. Rev.*, 1948, **73**, 360.
87 P. Barcellona and R. Passante, *Ann. Phys.*, 2015, **355**, 282.
88 G. L. Klimchitskaya and V. M. Mostepanenko, *Mod. Phys. Lett. A*, 2020, **35**(03), 2040007.
89 L. Novotny and C. Henkel, *Opt. Lett.*, 2008, **33**, 1029.
90 I. Yavuz, J. Schötz, M. F. Ciappina, P. Rosenberger, Z. Altun, M. Lewenstein and M. F. Kling, *Phys. Rev. A*, 2018, **98**, 043413.
91 V. Lozovski, V. Lysenko and N. Rusinchuk, *Sci. Rep.*, 2022, **12**, 17768.
92 J. H. K. Pfisterer, M. Baghernejad, G. Giuzio and K. F. Domke, *Nat. Commun.*, 2019, **10**(1), 5702.
93 V. Z. Lozovski, V. S. Lysenko and N. M. Rusinchuk, *Adv. Nat. Sci: Nanosci. Nanotechnol.*, 2020, **11**, 015014.
94 A. L. Suherman, G. Zampardi, S. Kuss, E. E. L. Tanner, H. M. A. Amin, N. P. Young and R. G. Compton, *Phys. Chem. Chem. Phys.*, 2018, **20**(14), 28300.
95 L. D. Burke and P. F. Nugent, *Gold Bull.*, 1997, **30**, 43.
96 C. Cardell and I. Guerra, *Sci. Adv.*, 2022, **9**(36), 8.
97 X. Ji, X. Song, J. Li, Y. Bai, W. Yang and X. Peng, *J. Am. Chem. Soc.*, 2007, **129**, 13939.
98 E. Nishikata, T. Ishii and T. Ohta, *J. Chem. Eng. Data*, 1981, **26**(3), 254.
99 X. Huang, L. Sheng, Y. Lu and S. Li, *Micromachines*, 2022, **13**(5), 771.
100 P. M. Boltovets, S. A. Kravchenko and B. A. Snopok, *Plasmonics*, 2010, **5**(4), 395.
101 C. N. Banwell and E. M. McCash, *Fundamentals of Molecular Spectroscopy*, McGraw-Hill, 1994.
102 R. C. Hilborn, *Am. J. Phys.*, 1982, **50**, 982.
103 O. Axner, J. Gustafsson, N. Omenetto and J. D. Winefordner, *Spectrochim. Acta, Part B*, 2004, **59**(1), 1.
104 W. E. Blass and G. W. Halsey, *Deconvolution of Absorption Spectra*, Academic Press, 1981.
105 W. F. Maddams, *Appl. Spectrosc.*, 1980, **34**(3), 245.
106 D. Applebaum, *Lévy Processes and Stochastic Calculus*, Cambridge University Press, 2009.
107 S. L. Li and D. G. Truhlar, *J. Chem. Theory Comput.*, 2017, **13**(6), 2823.
108 J. H. R. Clarke, in *Advances in Infrared and Raman Spectroscopy*, ed. R. J. H. Clark and R. E. Hester, 1978, vol. 4, p. 109.

109 T. Yatsui, M. Yamaguchi and K. Nobusada, *Prog. Quantum Electron.*, 2017, **55**, 166.
110 A. Al-Zubeidi, B. S. Hoener, S. S. E. Collins, W. Wang, S. R. Kirchner, S. a. H. Jebeli, A. Joplin, W. Chang, S. Link and C. F. Landes, *Nano Lett.*, 2019, **19**(2), 1301.
111 H. Bockmann, *"Far- and Near-Field Photochemistry of Single Molecules on a Metal Surface" PhDT*, 2019.
112 Y. Ohmi, S. Nishimura and K. Ebitani, *ChemSusChem*, 2013, **6**(12), 2259.
113 T. Yatsui, in *2017 OPJ-OSA Joint Symposia on Nanophotonics and Digital Photonics*, ed. T. Omatsu, OSA Technical Digest (online) Optica Publishing Group, 2017.
114 J. Hedberg, E. Blomberg and I. O. Wallinder, *Environ. Sci. Technol.*, 2019, **53**, 4030.
115 M. N. Martin, A. J. Allen, R. I. MacCuspie and V. A. Hackley, *Langmuir*, 2014, **30**(38), 11442.
116 D. E. Kim, J. Y. Kim, I. C. Sun, D. Schellingerhout, S. K. Lee, C. H. Ahn, I. C. Kwon and K. Kim, *Ann. Neurol.*, 2013, **73**(5), 617.
117 Y. Wang, J. E. Q. Quinsaat, T. Ono, *et al.*, *Nat. Commun.*, 2020, **11**, 6089.
118 V. Kesler, B. Murmann and H. T. Soh, *ACS Nano*, 2020, **14**(12), 16194.
119 E. T. Athira and J. Satija, *Analyst*, 2023, **148**, 6188.
120 B. A. Snopok and O. B. Snopok, in *Nanostructured Materials for the Detection of CBRN*, Springer, 2018.
121 S. İlday, G. Makey, G. B. Akgüç, Ö. Yavuz, O. Tokel, I. Pavlov, O. Gülseren and F. Ö. İlday, *Nat. Commun.*, 2017, **8**, 14942.
122 N. A. Kotov, *ACS Nano*, 2009, **3**(6), 1307.
123 M. Stöhr, M. Sadhukhan, Y. S. Al-Hamdani, J. Hermann and A. Tkatchenko, *Nat. Commun.*, 2021, **12**, 137.
124 T. Ocampo-Delgado and B. Ivlev, *J. Exp. Theor. Phys.*, 2010, **110**, 367.
125 A. Rao, S. Roy and P. P. Pillai, *Langmuir*, 2021, **37**(5), 1843.
126 H. M. Lee, Y. K. Kim, E. M. Go, C. Revadekar, K. H. Choi, Y. Cho, S. K. Kwak and B. J. Park, *Nat. Commun.*, 2023, **14**, 3838.
127 L. M. Woods, D. A. R. Dalvit, A. Tkatchenko, P. Rodriguez-Lopez, A. W. Rodriguez and R. Podgornik, *Rev. Mod. Phys.*, 2016, **88**, 045003.
128 R. Esquivel-Sirvent, *Physics*, 2023, **5**(1), 322.